Published in final edited form as:
Cancer Res. 2013 March 1; 73(5): 1524–1535. doi:10.1158/0008-5472.CAN-12-2796.

Acidity generated by the tumor microenvironment drives local invasion

Veronica Estrella[1,*], **Tingan Chen**[3,*], **Mark Lloyd**[3], **Jonathan Wojtkowiak**[1], **Heather H. Cornnell**[1], **Arig Ibrahim-Hashim**[1], **Kate Bailey**[1], **Yoganand Balagurunathan**[1], **Jennifer M. Rothberg**[4], **Bonnie F. Sloane**[5], **Joseph Johnson**[3], **Robert A Gatenby**[1,2], and **Robert J Gillies**[1,2]

[1]Department of Cancer Imaging and Metabolism; 12902 Magnolia Avenue; Tampa, Fl 33612

[2]Department of Radiology; 12902 Magnolia Avenue; Tampa, Fl 33612

[3]Department of Advanced Microscopy Laboratory H Lee Moffitt Cancer Center and Research Institute; 12902 Magnolia Avenue; Tampa, Fl 33612

[4]Cancer Biology Program, Wayne State University School of Medicine, Detroit, Michigan 48201

[5]Department of Pharmacology, Wayne State University School of Medicine, Detroit, Michigan 48201

Abstract

The pH of solid tumors is acidic due to increased fermentative metabolism and poor perfusion. It has been hypothesized that acid pH promotes local invasive growth and metastasis. The hypothesis that acid mediates invasion proposes that H+ diffuses from the proximal tumor microenvironment into adjacent normal tissues where it causes tissue remodeling that permits local invasion. In the current work, tumor invasion and peritumoral pH were monitored over time using intravital microscopy. In every case, the peritumoral pH was acidic and heterogeneous and the regions of highest tumor invasion corresponded to areas of lowest pH. Tumor invasion did not occur into regions with normal or near-normal pHe. Immunohistochemical analyses revealed that cells in the invasive edges expressed the glucose transporter GLUT-1 and the sodium-hydrogen exchanger NHE-1, both of which were associated with peritumoral acidosis. In support of the functional importance of our findings, oral administration of sodium bicarbonate was sufficient to increase peritumoral pH and inhibit tumor growth and local invasion in a preclinical model, supporting the acid-mediated invasion hypothesis.

Introduction

The propensity of cancers to invade adjacent normal tissues contributes significantly to local tumor growth and formation of metastases, which are largely responsible for tumor-associated morbidity and mortality (1). The mechanisms by which tumor cells invade are complex and can be modified in response to environmental conditions (2). Due to increased glucose metabolism, H^+ production and excretion are generally increased in cancers (3). This, combined with poor perfusion, results in an acidic extracellular pH (pHe) in malignant tumors (pH = 6.5 – 6.9) compared to normal tissue under physiologic conditions (pHe= 7.2 – 7.4) (4–6). Acidic pHe can induce release of (cysteine or aspartyl) cathepsin proteinase

Correspondence: Robert J. Gillies; robert.gilllies@moffitt.org.
*These authors contributed equally to this work

No relevant Conflicts of Interest

activity *in vitro* (7–9), which is generally believed to be involved in local invasion and tissue remodeling (10–12). Furthermore, cells exposed to *in vitro* low pH demonstrate increased invasion both *in vitro* and *in vivo* (9, 13, 14). These observations are synthesized in the "acid-mediated invasion" hypothesis, wherein H^+ ions flow along concentration gradients from tumor into adjacent normal tissue, promoting tissue remodeling at the tumor-stroma interface (15). The resulting acidic environment is toxic to normal cells, promotes a degradation of the extracellular matrix by proteinases (16), increases angiogenesis through the release of VEGF, and inhibits the immune response to tumor antigens (17–19). Cancer cells, because of their enhanced evolutionary capacity, develop adaptive mechanisms that allow them to survive and even proliferate in acidic environments (20). These adaptations can involve, *inter alia*, upregulation of the sodium-hydrogen exchange (NHE-1) or carbonic anhydrase (CA-IX) (21–23). As normal cells die and the extracellular matrix is degraded, cancer cells continue to proliferate and invade this open space. Thus, we propose that the acidic pH of the tumor microenvironment represents a "niche engineering" strategy that promotes local invasion and subsequent *in vivo* growth of malignant tumors. Support for this model has come from recent observations that neutralization of the tumor-derived acid with systemic buffers (e.g. bicarbonate, imidazole, lysine), can inhibit spontaneous and experimental metastases (8, 24, 25). Here we explicitly examine the acid-mediated invasion model by correlating regional variations in peritumoral acidity with subsequent patterns of tumor invasion.

An important tool to investigate acid-mediated invasion is the dorsal window chamber, first developed in 1987 (26). We have previously used this system to test aspects of the acid mediated invasion hypothesis, and have quantitatively measured the export of tumor-derived acid into surrounding stroma (16). Additionally, dorsal window chambers were used to observe a measureable decrease in tumor-stroma pH gradient following oral $NaHCO_3$ treatment, which has been shown to reduce formation of spontaneous or experimental metastases (8). In the current work, we observed that the acidic pHe of peritumoral tissues was coincident with the location of subsequent tumor invasion, which is a specific prediction of the "acid-mediated invasion" hypothesis. Furthermore, bicarbonate treatment reduced the pH gradient and prevented invasion completely. Thus, the current findings are directly supportive of the "acid-mediated invasion" hypothesis.

Materials and Methods

Animals

All animals were maintained under Institutional Animal Care and Use Committee (IACUC) at H. Lee Moffitt Cancer Center. Eight-to ten-week old severe combined immunodeficient (SCID) mice (22–25g, Charles River, Inc.) were used as host for MDA-MB-231/GFP, and HCT116/GFP tumors.

Cell Lines

In vitro and *in vivo* experiments were performed using three cells lines. All cell lines were passaged weekly in standard incubation conditions 37°C and 5% CO_2. Normal human mammary epithelial cells (HMEC - Invitrogen Life Technologies Corporation, Carisbad, CA) were maintained as adherent cultures in HuMEC Ready Medium (Invitrogen Life Technologies Corporation, Carisbad, CA). MDA-MB-231 cells (American Type Culture Collection, ATCC, Manassas, VA) were derived from a human breast cancer and HCT116 cells (American Type Culture Collection, ATCC, Manassas, VA), a human colon cancer cell line, were stably transfected with a pcDNA3 GFP vector following polyclonal selection. Green fluorescence was used in order to clearly distinguish tumor edge, to differentiate tumor from surrounding normal tissue and to accurately measure tumor growth. All three

cell lines were used for *in vitro* studies, however only the cancer cell lines were used *in vivo* for tumor development.

Extracellular Acidification Rate Measurement

Basal rates of extracellular acidification (ECAR) for HMEC, HCT116, and MDA-MB-231 cells were determined using the Seahorse Extracellular Flux (XF-96) analyzer (Seahorse Bioscience, Chicopee, MA). The XF-96 measures the rate of extracellular acidification in the medium above a monolayer of cells in real-time. This rate can be converted to a concentration of free protons using a measured buffering capacity. Cells (1.5×10^4/well) were seeded in a XF-96 microplate (V3-PET cat# 101104-004) in normal growth media overnight. One hour prior to measuring basal ECAR, the growth media was replaced with Seahorse assay media (cat# 100965-000) supplemented with 12.5mM D-Glucose, 0.5mM Sodium Pyruvate and 2mM L-Glutamine. Following flux measurements, protein concentrations were determined in situ for each well using a standard BCA protein assay (Thermo Scientific Pierce, Rockford, IL). Briefly, the wells were rinsed with Phosphate Buffer Solution (PBS) and stored at −80°C for 24 hours. The XF-96 microrplate was then thawed at room temperature upon which the BCA protein assay was performed directly in each well. Absorbance was determined at a wavelength of 560nm and mg protein was calculated using a set of standard BSA controls. ECAR values were normalized to mg/protein and were plotted as the mean +/− standard deviation.

Measurement of in vivo interstitial pH

HCT116 (GFP) or MDA-MB-231(GFP) cells were grown as subcutaneous tumors. Once tumors reached a volume > 800 mm^3, the extracellular pH was measured by microelectrode, as described previously (24). Briefly, pH measurements were obtained using an FE20 Five Easy pH meter (Mettler-Toledo, Colombus, OH). Animals were sedated with isoflurane (3.5%) prior to beginning the experiment, and remained under anesthesia (1.5–3.5% isoflurane) for the duration. A reference and pH electrode (MI-401F and MI-408B respectively, Microelectrodes Inc., Bedford, NH) were used to measure the pH by first inserting the reference electrode (OD 1mm) under the skin of the mouse near the tumor. The pH electrode (OD 0.8mm) was then inserted up to 1.3 cm into the center of each subcutaneous tumor. Electrodes were calibrated prior to and following each set of measurements using standard pH 7 and 10 buffers (Sigma, St. Louis MO). Two measurements were taken at each position and three positions were interrogated at each time point and averaged.

Dorsal Skin Window Chamber

Tumor constructs were engineered using the tumor droplet method (8). HCT116 (GFP) or MDA-MB-231(GFP) cells were suspended in 0.8 mg/ml of type 1 collagen (BD Bioscience #354249) and 1X DMEM at a final concentration of 2.5×10^6 cells/ml. Using a 48-well non-tissue culture plate, a 15-μl drop of the tumor suspension was polymerized in the center of the well. Polymerization occurred after 20–30min of incubation at 37°C. Following polymerization, the droplet was surrounded by a layer of type 1 collagen at a concentration of 1.25 mg/ml. This procedure allowed the tumors to maintain a circular shape with well defined borders. Following polymerization of the collagen (20–30min), the construct was incubated with 200μl of growth medium (DMEM with 10% fetal bovine serum) at 37°C. In parallel, a dorsal window chamber was implanted into recipient mice. After 2 days in culture the *in vitro* constructs were aseptically inoculated into the window chamber. Following 2–3 days of recovery, intravital images were acquired to assess tumor integrity and subsequent images were captured every 4–5 days to assess tumor growth and to develop a pH profile of the tumor microenvironment. To determine tumor volume, the GFP-expressing tumors were excited with an Argon laser tuned to 488 nm and emission was collected with a 498–538 nm

bandpass filter. Images were captured using an Olympus FV1000 MPE (multiphoton) microscope and analyzed using Image-Pro Plus v6.2 (Media Cybernetics; Bethesda, MD). At time of tumor regression, typically after 22–25 days (tumor dependent), intravital imaging was discontinued.

Ratiometric Measurements of Tumor pHe

Extracellular pH was measured using SNARF-1 Free Acid (Invitrogen #C-1270), a fluorescent pH indicator that exhibits a spectral shift in fluorescence emissions as a result of a change in pHe. pHe experiments were performed in window chambers prior to inoculation of tumor constructs in order to obtain accurate background measurements. Once a tumor was established, pHe measurements were again acquired. For SNARF measurements, mice were sedated with 1.5% isofluorane, covered with a warm pad to maintain appropriate body temperature and breathing was monitored during the duration of the imaging session. A tail vein injection of 200μl of 1mmol/L of SNARF-1 (free acid) solution was administered and diffusion into the tumor was observed by capturing images continuously for the first 15 minutes using the confocal modality of an Olympus FV1000 MPE. Further images were captured at 30, 40, 50 and 60 minutes post SNARF-1 injection. Spatial distribution of pHe in the tumor and adjacent normal tissue was obtained by exciting the dye with a He/Ne laser at 543nm and emissions were collected with a 570–620 nm bandpass filter and with a 640 nm long pass filter. Confocal images from each channel were converted to .tif format using Imaris software, followed by the subtraction of background from each fluorescence image and smoothing with a 7 × 7 kernel with Image-Pro Plus v6.2. Ratiometric images were produced by applying algorithms to the smoothed images using the Definiens Developer XD 1.5. Every ratiometric pixel was used to convert to a pH value by applying *in vitro* calibration data. The pH was calculated using the equation:

$$pH=pKa - \log[((R - R_B)/(R_A - R)) \times ((F\,B(\lambda 2))/(F\,A(\lambda 2)))]. \quad \text{Eqn 1}$$

where R is the ratio of emissions from the 2 channels, R_A is the maximal ratio (observed at acidic endpoint); R_B is the minimal ratio (observed at the alkaline endpoint), and ((F B(λ2))/(F A(λ2))) is a correction factor for the ratio of fluorescence values (F) between alkaline (B) and acidic (A) endpoints at the higher wavelength(27). At 1.25× R_A=1.863; R_B=0.954 and 4× R_A=1.725; R_B=0.966. To determine the pH in different tumor regions and the area adjacent to the tumor, radial lines emanating from the tumor centroid were drawn and average pH distribution along the lines was determined. “0” was assigned as the tumor centroid, and pH images were aligned so that they coincided at the tumor margin using the GFP image to determine the tumor edge.

In vitro Collagen I and Collagen IV degradation

Collagen degradation was measured by the increase in fluorescence of Dye-Quenched (DQ-) collagen I and collagen IV (Life Technologies Corp) according to methods described in (28). For DQ-collagen I, 6 well tissue culture plates were coated with 600 μl of 1.25 mg/mL of type 1 rat tail collagen (BD Bioscience) containing 25mg/ml of DQ-collagen I and placed in a 37 °C incubator for 30 min to allow for polymerization. For DQ-collagen IV, glass coverslips in 35 mm dishes were coated with 45 μl of Cultrex (Trevigen) containing 25 mg/ml of DQ-collagen IV and placed in a 37 °C incubator for 10 min to allow for polymerization. Cells were labeled with 10μM Cell Tracker Orange (Life Technologies, Corp) and approximately 40,000 or 2500 cells were seeded on top of the collagen or Cultrex, respectively, and incubated at 37°C for 30–60 min until adherent, at which point either a neutral or acidic culture medium was applied. To visualize cell nuclei, cells were incubated with 5μg/ml of Hoechst (Molecular Probes) for 10 min at 37°C. All images were obtained with a Leica TCS SP5 AOBS laser scanning confocal microscope through a 20X/0.7NA

Plan Apochromat objective lens (Leica Microsystems, Germany). 405 Diode, Argon 488 and HeNe 543 laser lines were applied to excite the samples and tunable emissions were used to minimize crosstalk between fluorochromes. Image z-sections for each sample were captured with photomultiplier detectors and prepared with the LAS AF software version 2.6 (Leica Microsystems, Germany). A 2× zoom was applied to increase the total magnification to 400×. Analysis of DQ-Collagen in the z-stack images was performed using Definiens® Developer v1.5 (Definiens, Munich, Germany) software suite. First the intracellular area was determined with automatic threshold segmentation on the combination of Hoechst stain and Cell Tracker Red. The intracellular segmentation was performed on all sections of the z-stack and connected in three dimensions. Total pixel area was extracted from this intracellular segmentation. Next contrast split segmentation with a minimum threshold of 50 grayscale values was used to segment DQ collagen stain from background. The DQ collagen segmentation was also performed on all sections and connected in three dimensions. Finally the localization (intracellular vs. extracellular) of DQ-Collagen was determined based on the initial intracellular segmentation, mentioned above, and the fluorescence signal from the DQ-Collagen was normalized by the intracellular total pixel area.

In vivo vessel density

Images were acquired with 488nm excitation with a 1.25× lens with GFP (tumor) and transmitted light emissions. The GFP expressing tumor images were subtracted from the transmitted light images leaving a 0 intensity (black) value in place of the tumor. The center of mass for each tumor at early (day4) and late (day13) timepoints were identified (white dot). Four quadrants were drawn radiating 3mm from the tumor centroid. Each image was brightfield flattened (20pxl width). The darker vessels were identified by an open object threshold between 1–75 dynamic range units for this 8bit image (0 is excluded to avoid the subtracted tumor). ROIs were placed in each quadrant and the area of the vessels was quantified in pixels. The area of the tumor (pixels) was also quantified in each quadrant. Tumor growth was considered the area of tumor in Day13 subtracted from the area of tumor in Day4. This data was graphically plotted against the early vessel density (area in pixels) from the Day4 time point.

Bicarbonate treatment

Before initiating the $NaHCO_3$ treatment, animals were randomly divided into control (n=4) and experimental (n=8) groups. Six days prior to the inoculation of the tumor constructs into the dorsal window chamber, the control group drank tap water and the experimental group was provided with 200 (mM) of $NaHCO_3$ *ad libitum*. Three days prior to the inoculation of the tumor constructs, the dorsal window chambers were implanted and a day before the inoculation, pHe Images were acquired to use as background measurements. $NaHCO_3$ treatment continued throughout the course of the experiment. Once the experiment was terminated, xenografted tissues were collected and analyzed *ex vivo* by histology and immunohistochemistry.

Immunohistochemistry (IHC)

Once imaging sessions were completed, the xenografted tumors were harvested, fixed in 10% Neutral Buffered Formalin (Thermo Scientific) for 24 hours, processed and embedded in paraffin. Routine hematoxylin and eosin (H & E) stains were performed on 4 μm sections of tissue. Na^+/H^+ Exchanger −1 (NHE-1), Glucose Transporter-1 (GLUT1), and CD31 were detected by immunohistochemistry using the Ventana Discovery XT automated system (Ventana Medical Systems, Tucson, AZ). Rabbit polyclonal NHE-1 antibody (#sc-28758, Santa Cruz Biotechnology, Santa Cruz, CA) was incubated at a dilution of 1:200; rabbit polyclonal Glut-1 antibody and rabbit polyclonal CD31 antibody (#ab15309 and #ab28364 Abcam, Cambridge, MA) were incubated at a dilution of1:400. All antibodies were

incubated for 32 min in Dako antibody diluent (Carpenteria, CA), followed by a 20-minute incubation in Ventana OmniMap Anti-Rabbit Secondary Antibody and detected with the Ventana ChromoMap kit system.

Results

Cancer cells have enhanced rates of glucose metabolism which produces an acidic environment that may promote degradation of the stromal extracellular matrix and local invasion. The basal rate of proton production is a proximal component in this acidity. In the process of generating ATP, cells produce H^+ through both oxidative phosphorylation and glycolysis. Rates of proton production were determined in normal human mammary epithelial (HMEC) cells, and established colon (HCT116) and breast (MDA-mb-231) cancer cell lines, as shown in Figure 1A. These data show that HCT116 had significantly higher rates of extracellular acidification ($P<0.001$), compared to HMEC and MDA-mb-231. MDA-mb-231 also produced H^+ at a significantly higher rate compared to HMEC. Thus, the acid production rates of both cancer lines were higher compared to normal epithelial cells, which is a common observation (5, 6, 29, 30). Notably, these data were normalized to protein, and HCT116 are much smaller than either of the breast lines so that H^+ production rates of HCT116 was comparable to that of MDA-mb-231, on a *per cell* basis (supplemental figures S1,2),

The higher rates of acid production by HCT116 would predict that tumors of these cells would have a lower steady state pHe, compared to MDA-mb-231 tumors. To investigate this, tumor cells were injected subcutaneously into SCID mice and allowed to reach a tumor volume of 1000 mm^3. Once the desired volume was reached, a pH-sensitive microelectrode system was used to measure the pHe of these tumors in multiple locations ($n = 9$ for HCT-116 and $n=7$ for MDA-mb-231). These measurements indicated a significantly ($P<0.01$) more acidic pHe within the HCT116 tumors as compared to MDA-MB-231 tumors (Figure 1B). Thus, these *in vivo* tumor data are consistent with the *in vitro* proton production measurements. Both *in vitro* and *in vivo* evaluations suggest that the HCT116 cells created a more acidic extracellular environment which may be an important factor in the development of a more aggressive tumor phenotype.

The next step in evaluating the extracellular tumor microenvironment was to monitor tumor growth within the dorsal window chamber, DWC. Prior to *in vivo* testing, we optimized collagen matrix concentrations for *in vitro* growth and observed that a concentration of 0.8 mg/mL supported maximal *in vitro* growth for both cell lines (data not shown). Following *in vivo* implantation in optimized matrixes, we observed that HCT116 xenografts grew rapidly and reproducibly, with a significant ($p<0.0001$) 95% increase in tumor-associated pixels by day 16 (Figure 1C). In contrast, the MDA-mb-231 tumors grew more slowly, i.e. a 37% increase in tumor area by day 16 (supplemental figure S3). These basal growth experiments also allowed us to identify the optimum time to observe tumor growth and invasion. Intravital microscopy images of the tumor and its microenvironment can normally be captured for up to a month before skin retraction of the DWC is observed. Thus, we limited our observation window to 3 weeks, wherein we considered tumor growth would be unimpeded by failure of the dorsal flap. Notably most observations were made prior to 15 days of inoculation (Figures 1,2). Figure 1D shows four different HCT116/GFP tumors early (day 2–4) and late (day 10–13) during tumor growth, illustrating the increase in the physical size of the tumor within the chamber and that the growth was directionally heterogeneous. In the initial days of imaging, the HCT116/GFP tumors maintained their original circular morphology. By day 16, the tumors had approximately doubled their original size (Figure 1C). The early and late images were pseudo-colored in order to superimpose the images and illustrate that tumors grew anisotropically the dorsal window chamber.

We have previously proposed that a decrease in the pH of the microenvironment might pose a growth advantage to tumors because of their ability to resist acid-induced cellular toxicity. Figure 1D illustrates the growth that took place within the window chamber within the first two weeks of inoculation. In order to relate growth to the pH of the extracellular peritumoral environment, SNARF-1 free acid was used to map the pH of the tumor and its surrounding microenvironment. Representative ratiometric results are shown in Figure 2A and show that anisotropically distributed decreases in pHe in both the tumor and neighboring environment were observable by day 7. By day 14, acidic regions were distinct and easily identifiable, specifically in the regions into which the tumor had grown (Figure 2B). Superimposing the green and red images showed that the tumor invaded the normal tissue that was most acidic. In order to investigate the relationship between the direction of acidity and path of invasion, the peritumoral pH and direction of tumor growth were more deeply analyzed, as shown in Figure 2C. First, the center-of-gravities, COG, for both the day 4 and day 14 tumors were determined, and they were then co-registered using the rim of the window chamber as a fiducial marker. The ratiometric images were also co-registered and the peritumoral pH was measured in an area that spanned 100 microns from the tumor edge. Both tumor growth and pH were measured at every 22.5 degrees of arc from the COG. Tumor growth was quantified as the number of pixels between edges of the tumor on days 4 and 14 (Figure 2C and supplemental Figure S4), allowing us to compare growth and pHe. As a result, we were able to identify that the direction towards which the tumor grew by day 14 was also the predominant area of acidification. In this particular tumor, taking into consideration that 0° was “true west” relative to the ring clip of the dorsal window chamber, maximal tumor growth and the greatest acidity both occurred at 45° (arrows in Figures 2B). The entire radial relationship between peritumoral pH and tumor growth is shown in Figure 2D. The vertical dotted line in the graph represents maximal growth and minimal pH occurring coincidentally at 45°. In regions where the normal tissue had a more alkaline pH, little or no invasion was observed. This pattern was observed across all five tumors in this study, wherein growth was highly correlated ($p<0.02$) with acidic pH below a threshold that varied from pH 6.8–7.1 in individual mice (Supplemental Figure S5). This variability in threshold is expected due to inaccuracies in assigning scalar pH values using ratiometric methods (27). To address the question: “Is growth greatest in areas with lowest pH?”, we compared the growth in the volumes with the highest and lowest terciles of pH values for each mouse. Across individual mice, the t-test p-values were 0.003, 0.07, 0.006, 0.12 and 0.008. Across all mice, the difference in growth between low and high pH volumes had a p-value of 4e-9.

Following the final image acquisition, the mice were sacrificed and the tumors were removed from the chamber and immediately fixed for histology. In order to better understand the underlying biology of this regional acidosis and tumor growth, *ex vivo* biomarker analyses were performed to determine the expression and spatial distribution of metabolic and angiogenic tumor markers such as the glucose transporter, GLUT-1, the sodium hydrogen exchanger, NHE-1, and the endothelial marker, CD31. It was reasoned that GLUT-1 and NHE-1 work coordinately to acidify the extracellular environment. As shown in Figure 3A, there was a higher level of GLUT-1 expression at the tumor edge compared to the core. Since GLUT-1 levels are correlated to high glycolysis (31) and high glycolysis is correlated to acid production (3), this regional heterogeneity of GLUT-1 expression was consistent with the lower pHe at the tumor edge (cf. Figure 2A). Cancer cells adapt to low pHe by upregulating membrane transporters, which help maintain intracellular pH. One of these transporters is NHE-1, which showed a similar regional pattern of overexpression compared to GLUT-1. Image analysis software was used to more accurately characterize these expression profiles. For these analyses, individual cells were identified by nuclei and segmented and the expression level of each IHC marker was then quantified and expressed on a per-cell basis. These expression levels were then normalized to radial position, from the edge to the center of the tumor. Figure 3B shows that NHE-1 normalized

expression levels were highest at the tumor edge, whereas maximal expression of GLUT-1 was approximately 100μm from the edge. This pattern was statistically significant and was observed consistently across all four preparations in this study, as shown by the trend graph (Figure 3C). These results are consistent with the acidification shown in the peritumoral region in Figure 2A and 2B.

Figure 4A shows high-resolution IHC images of localized micro-invasion at the tumor-host interface. The large arrows in the figure denote the region of invasion and smaller arrows designate the tumor host interface. As above, high expression of GLUT-1 and NHE-1 were localized to tumor cells in this invasive region, in contrast to the vessel marker, CD31, which was elevated in the adjacent (reactive) stroma. In order to more deeply quantify the expression of these markers, staining levels were expressed on a per-cell basis (Figure 4B), wherein red, orange and yellow were used to demark strong, moderate and weak uptake, respectively. Deeper analysis of CD31 expression showed that vessel density was significantly ($p<0.05$) higher in reactive stroma, compared to the tumor or distant stroma (Supplemental Figure S6). These findings suggested that both GLUT-1 and NHE-1 were localized at the tumor front and at regions of localized invasion, consistent with the decrease in pH observed in the *in vivo* chamber studies. The presence of CD31 positive vessels in the reactive stroma may act as a sink for the tumor derived acids, and thus would limit the penetration of the acidification deeper into the stroma. Although at lower resolution compared to *ex vivo* data, spatial analyses of vessel density *in vivo* showed significant radial heterogeneity in peri-tumoral regions (Supplemental Figure S7). When these data were compared to spatially explicit invasive growth, it appeared that there was an inverse relationship between vessel density and tumor growth (Supplemental Figure S8). These observations were also consistent with the invasion into areas of lower pH, as the more poorly perfused regions can be expected to be more acidic.

Prior work has suggested that acidic pH conditions can stimulate the release of cysteine cathepsins (8) and increase levels of activated collagenases (32). To investigate this, *in vitro* studies measured the effect of culture pH on proteolytic activity of HCT116 cells grown in matrixes containing dye-quenched (DQ) collagens I or IV, using methods previously described (28). Collagens I and IV were interrogated because collagen I was used in the DWC system and collagen IV is found in basement membrane. Proteolytic activity was assessed using confocal microscopy and analyzed using Definiens Derveloper v1.5. These data showed collagen degradation was significantly higher at pH 6.8, compared to 7.4 in HCT116 cultures (Supplemental Figure S9). This is identical to results observed for MDA-mb-231 cells using the same system (Rothberg et al., unpublished). While these data do not identify the exact mechanism by which acidity promotes invasion, they do indicate that the mechanism involves the production, release and/or activation of matrix degrading proteases.

Although the above data are consistent with acid-mediated invasion, it remains a possibility that the acid pH is a consequence, and not a cause, of invasion. To test this, the tumor pH was neutralized using a systemic pH buffer, sodium bicarbonate. We have previously shown that a variety of buffers including bicarbonate, Tris, Lysine and imidazoles, can neutralize tumor pHe and inhibit tumor invasion and metastasis (8, 24). In this current study, window chamber-bearing mice were randomized into control (tap water) and bicarb (200mM *ad lib.*) groups, which continued for the duration of the experiment. After 6 days of acclimation, the window chambers were inoculated with HCT116/GFP droplet constructs and the tumors monitored as above. Intravital images were captured two days after inoculation to examine integrity of the tumor and to capture initial pHe measurements. After 2 days, there were no differences in the size or density of inoculated tumors between the two groups. Monitoring of tumor growth and pHe levels was continued throughout the experiment every 4–5 days. As shown on Figure 5A, tumors treated with bicarbonate displayed a different growth

pattern than the controls (cf. Figure 1D). Figure 5B shows that the control tumors almost doubled in volume by day 13, whereas the volumes of $NaHCO_3$ treated tumors were not significantly changed between days 1 and 13. Inhibition of growth by bicarbonate was highly significant, as shown in supplemental Figure S10 ($p<0.02$). Figure 5C shows the pH values mapped within the chamber on both day 8 and day 19 post inoculation, and demonstrated that pHe of the tumor and its microenvironment were higher in the bicarbonate group compared to controls (cf. Figure 2A). Using calibration data, the ratiometric data were converted into scalar pH values, and the intratumoral and peritumoral pH values of the bicarbonate and control tumors were obtained. Measurements were calculated using all intravital images per group along 4 radial directions (Figure 6A and 6B). The mean values were plotted to show a pH gradient from the center of the tumor to the tumor edge, and from the tumor edge into and across the stromal extracellular matrix adjacent to each tumor (Figure 6C and D). The pH values for all control and bicarbonate tumors were collected and mean measurements were plotted. By day 15 post-inoculation, there were no significant differences in the pH values at the centers of the tumors for control ($pH=6.78 \pm 0.25$) and bicarbonate-treated ($pH = 6.97 \pm 0.15$) tumors. In contrast, the pH at the edge of control tumors were significantly ($p<0.05$) more acidic ($pH = 6.75 \pm 0.19$ SD) compared to that of bicarbonate treated tumors ($pH = 7.14 \pm 0.05$). These results show that, in a window chamber model, systemic buffering with $NaHCO_3$ increased the peritumoral pH and reduced local invasion.

Discussion

The morbidity and mortality associated with cancer is largely related to tumor invasion and formation of metastases. Extensive application of FDG-PET imaging to clinical cancers has clearly demonstrated the vast majority of malignant tumors metabolize glucose at high rates. (33, 34). We propose there is a direct, causative link between increased glucose metabolism and the ability of cancer cells to invade and metastasize.

Elevated glucose metabolism is the proximate cause of increased acidity in the tumor microenvironment. Furthermore, most tumors develop an aberrant vasculature network that tends to be poorly organized and leaky, disrupting blood flow and hampering the delivery of oxygen. (35). This has a two-fold effect on tumor acidity. First, it subjects tumor regions to poor perfusion and hence, poor oxygenation (36). Low oxygenation increases glycolytic flux via the Pasteur Effect (37). Notably, even in tumor regions with adequate oxygen supply, glycolysis and acid production are up regulated via the Warburg Effect (38). Second, poor perfusion hampers the ability of the microenvironment to remove tumor derived acid through diffusion. Consequently, the extracellular pH of tumors is typically highly acidic, and this will inevitably result in acid diffusion into the surrounding stroma.

We have previously proposed that the invasive phenotype and increased glucose metabolism are, in fact, closely linked (23). Much of this work stems from viewing cancer biology as an ecological and evolutionary process. Within this context, all commonly observed phenotypes in cancers must be confer an evolutionary advantage. In this case we ask “how does increased glucose metabolism and consequent interstitial acidosis confer an evolutionary advantage that promotes tumor cell proliferation”? This has led to the proposal that regional acidosis represents a strategy commonly observed in nature as “niche engineering” in which plants and animal alter their environment in ways that promote their own growth and survival and/or diminishes that of their competitors. The conceptual model that tumors use increased glucose metabolism, even in the presence of adequate oxygen, as a form of niche engineering is the basis of the “acid mediated invasion” hypothesis (15, 16). The model assumes that through evolutionary events during carcinogenesis, as cancer cells proliferate on epithelial surfaces (39), they must adapt to increased acid production by

expression of proton export systems, such as NHE-1 or CA-IX, which transport H^+ from intra- to extracellular space, resulting in extracellular acidification. However, normal mammalian tissue, lacking the evolutionary capacity of cancer cells, typically remains intolerant of prolonged exposure to acidic pH. This model posits H^+ flows along concentration gradients, from the tumor into the peritumoral normal tissue, causing disruption that favors subsequent tumor growth. A variety of studies have shown that an acidic peritumoral pH is associated with a degradation of the extracellular matrix, possibly through the release and activation of proteolytic enzymes (7, 16). The low pH also leads normal cells to undergo apoptosis and necrosis while cancer cells survive due to acquired resistance mechanisms (40, 41). In summary, regional acidosis causes substantial niche engineering through normal cell death, breakdown of extracellular matrix, promotion of new vessel formation, and suppression of the immune response (10, 17, 18).

The results of this study suggest that tumor cells do, indeed, perform niche engineering by creating an acidic environment that is non-toxic to the malignant cells but, through its negative effects on normal cells and tissue, promotes local invasion. Targeting this evolutionary strategy through systemic buffers and other mechanisms to reduce peri-tumoral pH will likely provide a valuable adjunct or alternative to traditional therapies focused entirely on killing the tumor cells.

Supplementary Material

Refer to Web version on PubMed Central for supplementary material.

Acknowledgments

U54 CA143970 (RAG and RJG); R01 CA 077575 (RJG and RAG); R01 CA 131990S (BFS and JMR)

References

1. Ruoslahti E. How cancer spreads. Sci Am. 1996; 275(3):72–77. [PubMed: 8701296]
2. Friedl P, Wolf K. Tumour-cell invasion and migration: diversity and escape mechanisms. Nature reviews Cancer. 2003; 3(5):362–374.
3. Schornack PA, Gillies RJ. Contributions of cell metabolism and H+ diffusion to the acidic pH of tumors. Neoplasia. 2003; 5(2):135–145. [PubMed: 12659686]
4. Stubbs M, McSheehy PM, Griffiths JR, Bashford CL. Causes and consequences of tumour acidity and implications for treatment. Mol Med Today. 2000; 6(1):15–19. [PubMed: 10637570]
5. Gillies RJ, Liu Z, Bhujwalla Z. 31P-MRS measurements of extracellular pH of tumors using 3-aminopropylphosphonate. The American journal of physiology. 1994; 267(1 Pt 1):C195–C203. [PubMed: 8048479]
6. van Sluis R, Bhujwalla ZM, Raghunand N, et al. In vivo imaging of extracellular pH using 1H MRSI. Magnetic resonance in medicine : official journal of the Society of Magnetic Resonance in Medicine / Society of Magnetic Resonance in Medicine. 1999; 41(4):743–750. [PubMed: 10332850]
7. Rozhin J, Sameni M, Ziegler G, Sloane BF. Pericellular pH affects distribution and secretion of cathepsin B in malignant cells. Cancer Res. 1994; 54(24):6517–6525. [PubMed: 7987851]
8. Robey IF, Baggett BK, Kirkpatrick ND, et al. Bicarbonate increases tumor pH and inhibits spontaneous metastases. Cancer Res. 2009; 69(6):2260–2268. [PubMed: 19276390]
9. Rofstad EK, Mathiesen B, Kindem K, Galappathi K. Acidic extracellular pH promotes experimental metastasis of human melanoma cells in athymic nude mice. Cancer Res. 2006; 66(13):6699–6707. [PubMed: 16818644]
10. Chambers AF, Matrisian LM. Changing views of the role of matrix metalloproteinases in metastasis. J Natl Cancer Inst. 1997; 89(17):1260–1270. [PubMed: 9293916]

11. Sloane BF, Moin K, Krepela E, Rozhin J. Cathepsin B and its endogenous inhibitors: the role in tumor malignancy. Cancer Metastasis Rev. 1990; 9(4)
12. Rochefort H, Liaudet-Coopman E. Cathepsin D in cancer metastasis: a protease and a ligand. Apmis. 1999; 107(1):86–95. [PubMed: 10190284]
13. Moellering RE, Black KC, Krishnamurty C, et al. Acid treatment of melanoma cells selects for invasive phenotypes. Clinical & experimental metastasis. 2008; 25(4):411–425. [PubMed: 18301995]
14. Schlappack OK, Zimmermann A, Hill RP. Glucose starvation and acidosis: effect on experimental metastatic potential, DNA content and MTX resistance of murine tumour cells. Br J Cancer. 1991; 64(4):663–670. [PubMed: 1911214]
15. Gatenby RA, Gawlinski ET. A reaction-diffusion model of cancer invasion. Cancer Res. 1996; 56(24):5745–5753. [PubMed: 8971186]
16. Gatenby RA, Gawlinski ET, Gmitro AF, Kaylor B, Gillies RJ. Acid-mediated tumor invasion: a multidisciplinary study. Cancer Res. 2006; 66(10):5216–5223. [PubMed: 16707446]
17. Fukumura D, Xu L, Chen Y, Gohongi T, Seed B, Jain RK. Hypoxia and acidosis independently up-regulate vascular endothelial growth factor transcription in brain tumors in vivo. Cancer Res. 2001; 61(16):6020–6024. [PubMed: 11507045]
18. Xu L, Fukumura D, Jain RK. Acidic extracellular pH induces vascular endothelial growth factor (VEGF) in human glioblastoma cells via ERK1/2 MAPK signaling pathway: mechanism of low pH-induced VEGF. The Journal of biological chemistry. 2002; 277(13):11368–11374. [PubMed: 11741977]
19. Lardner A. The effects of extracellular pH on immune function. Journal of leukocyte biology. 2001; 69(4):522–530. [PubMed: 11310837]
20. Jonathan Wojtkowiak JMR, Virendra Kumar, Schramm Karla J, Haller Edward, Proemsey Joshua B, Lloyd Mark C, Sloane Bonnie F, Gillies Robert J. Chronic autophagy is a cellular adaptation to tumor acidic pH microenvironments. Cancer Res. 2012 Published OnlineFirst June 19, 2012.
21. Chiche J, Ilc K, Laferriere J, et al. Hypoxia-inducible carbonic anhydrase IX and XII promote tumor cell growth by counteracting acidosis through the regulation of the intracellular pH. Cancer Res. 2009; 69(1):358–368. [PubMed: 19118021]
22. Ivanov S, Liao SY, Ivanova A, et al. Expression of hypoxia-inducible cell-surface transmembrane carbonic anhydrases in human cancer. The American journal of pathology. 2001; 158(3):905–919. [PubMed: 11238039]
23. Gatenby RA. The potential role of transformation-induced metabolic changes in tumor-host interaction. Cancer Res. 1995; 55(18):4151–4156. [PubMed: 7664293]
24. Ibrahim Hashim A, Cornnell HH, Coelho Ribeiro Mde L, et al. Reduction of metastasis using a non-volatile buffer. Clinical & experimental metastasis. 2011; 28(8):841–849. [PubMed: 21861189]
25. Ibrahim-Hashim A, Cornnell HH, Abrahams D, et al. Systemic Buffers Inhibit Carcinogenesis in TRAMP Mice. J Urol. 2012
26. Dewhirst MW, Gustafson C, Gross JF, Tso CY. Temporal effects of 5.0 Gy radiation in healing subcutaneous microvasculature of a dorsal flap window chamber. Radiat Res. 1987; 112(3):581–591. [PubMed: 3321144]
27. Martinez-Zaguilan R, Martinez GM, Lattanzio F, Gillies RJ. Simultaneous measurement of intracellular pH and Ca2+ using the fluorescence of SNARF-1 and fura-2. The American journal of physiology. 1991; 260(2 Pt 1):C297–C307. [PubMed: 1996613]
28. Jedeszko C, Sameni M, Olive MB, Moin K, Sloane BF. Visualizing protease activity in living cells: from two dimensions to four dimensions. Current protocols in cell biology / editorial board, Juan S Bonifacino [et al. 2008; Chapter 4(Unit 4):20.
29. Huber V, De Milito A, Harguindey S, et al. Proton dynamics in cancer. Journal of translational medicine. 2010; 8:57. [PubMed: 20550689]
30. Wike-Hooley JL, Haveman J, Reinhold HS. The relevance of tumour pH to the treatment of malignant disease. Radiotherapy and oncology : journal of the European Society for Therapeutic Radiology and Oncology. 1984; 2(4):343–366. [PubMed: 6097949]

31. Bos R, van Der Hoeven JJ, van Der Wall E, et al. Biologic correlates of (18)fluorodeoxyglucose uptake in human breast cancer measured by positron emission tomography. J Clin Oncol. 2002; 20(2):379–387. [PubMed: 11786564]
32. Martinez-Zaguilan R, Seftor EA, Seftor RE, Chu YW, Gillies RJ, Hendrix MJ. Acidic pH enhances the invasive behavior of human melanoma cells. Clinical & experimental metastasis. 1996; 14(2): 176–186. [PubMed: 8605731]
33. Gambhir SS. Molecular imaging of cancer with positron emission tomography. Nature reviews. 2002; 2(9):683–693.
34. Basu S, Chen W, Tchou J, et al. Comparison of triple-negative and estrogen receptor-positive/progesterone receptor-positive/HER2-negative breast carcinoma using quantitative fluorine-18 fluorodeoxyglucose/positron emission tomography imaging parameters: a potentially useful method for disease characterization. Cancer. 2008; 112(5):995–1000. [PubMed: 18098228]
35. Jain RK. Tumor angiogenesis and accessibility: role of vascular endothelial growth factor. Seminars in oncology. 2002; 29(Suppl 16)(6):3–9. [PubMed: 12516032]
36. Dewhirst MW, Secomb TW, Ong ET, Hsu R, Gross JF. Determination of local oxygen consumption rates in tumors. Cancer Res. 1994; 54(13):3333–3336. [PubMed: 8012945]
37. Racker E. History of the Pasteur effect and its pathobiology. Molecular and cellular biochemistry. 1974; 5(1–2):17–23. [PubMed: 4279327]
38. Semenza GL, Artemov D, Bedi A, et al. 'The metabolism of tumours': 70 years later. Novartis Foundation symposium. 2001; 240:251–260. discussion 60-4. [PubMed: 11727934]
39. Gatenby RA, Gillies RJ. Why do cancers have high aerobic glycolysis? Nature reviews. 2004; 4(11):891–899.
40. Williams AC, Collard TJ, Paraskeva C. An acidic environment leads to p53 dependent induction of apoptosis in human adenoma and carcinoma cell lines: implications for clonal selection during colorectal carcinogenesis. Oncogene. 1999; 18(21):3199–3204. [PubMed: 10359525]
41. Park HJ, Lyons JC, Ohtsubo T, Song CW. Acidic environment causes apoptosis by increasing caspase activity. Br J Cancer. 1999; 80(12):1892–1897. [PubMed: 10471036]

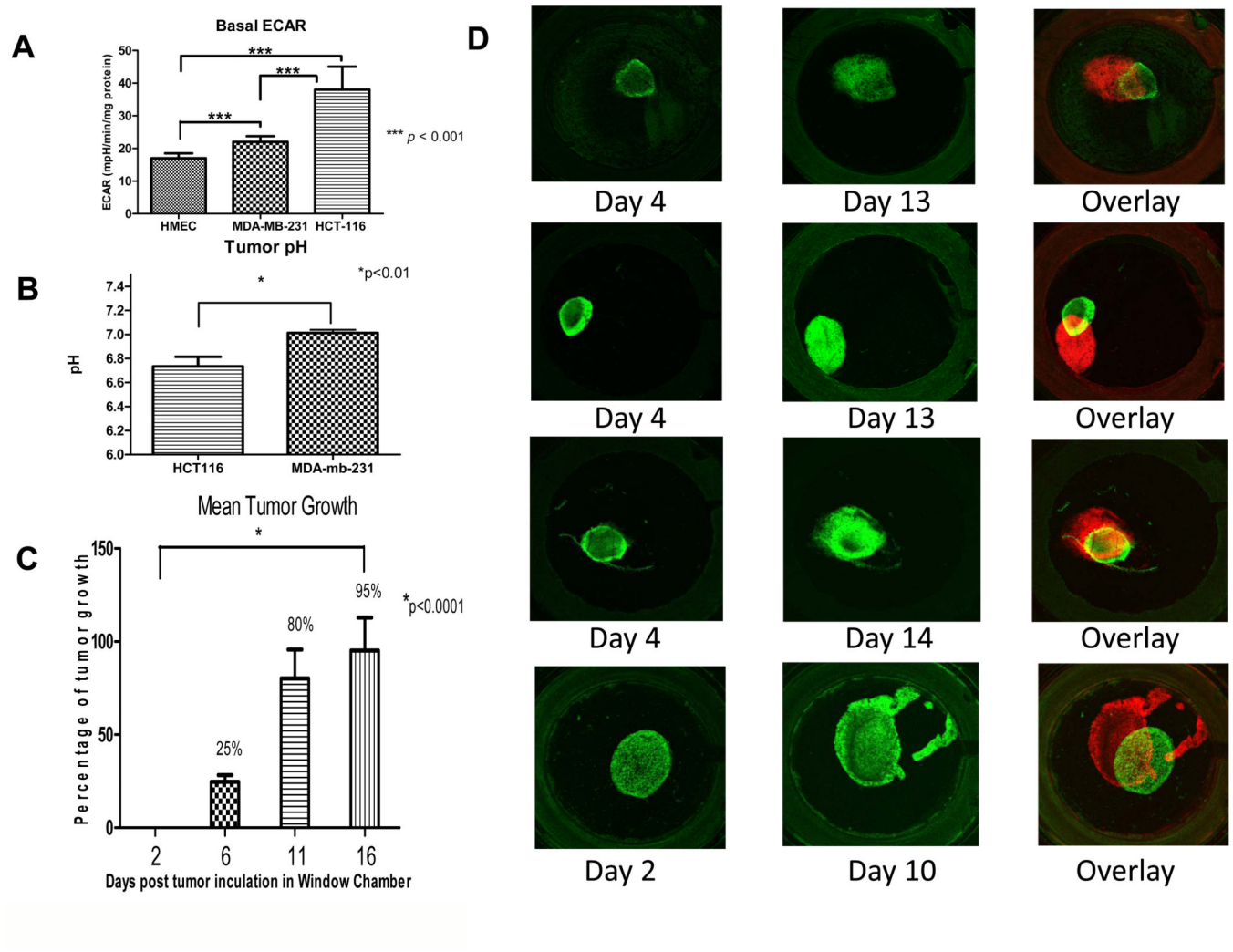

Figure 1. Proton production, pHe and tumor growth

(A) *In vitro* extracellular acidification rate, ECAR, of tumor cells *vs.* normal cells. The rate of proton production was determined over a 30 minute time period using Seahorse XF-96 Instrument designed to measure *in vitro* metabolic rates. We show a significant increase in H^+ production especially in our colon cancer cell line HCT116 when compared to human normal mammary epithelial cells HMEC (*P<0.001). (B) *In vivo* pH tumor measurements. Tumor pH measurements were obtained by electrode. The average pH of the tumors for each cell line are shown, with a significantly (*P<0.01) lower pHe in the HCT116, compared to MDA-mb-231, tumors. (C) Mean growth of HCT116/GFP tumors within the dorsal window chamber. Tumor area was measured at days 2, 6, 11 and 16 by fluorescent pixel number. Data are expressed as *percent increase* by the ratio of area at given day to that of day 2 and subtracting 100 for normalization. Thus, a 100 percent increase represents a doubling of area. The mean growth illustrated a significant increase in size of the tumor over 2 weeks (p<0.0001). (D) Intravital microscopy images of *in vivo* tumor growth in the dorsal window chamber. The images were captured with a 1.25X lens on days 2 or 4 and 10, 13 or 14. These longitudinal images were pseudo-colored green (early) or red (late) in order to superimpose the images and observe magnitude and direction of tumor growth.

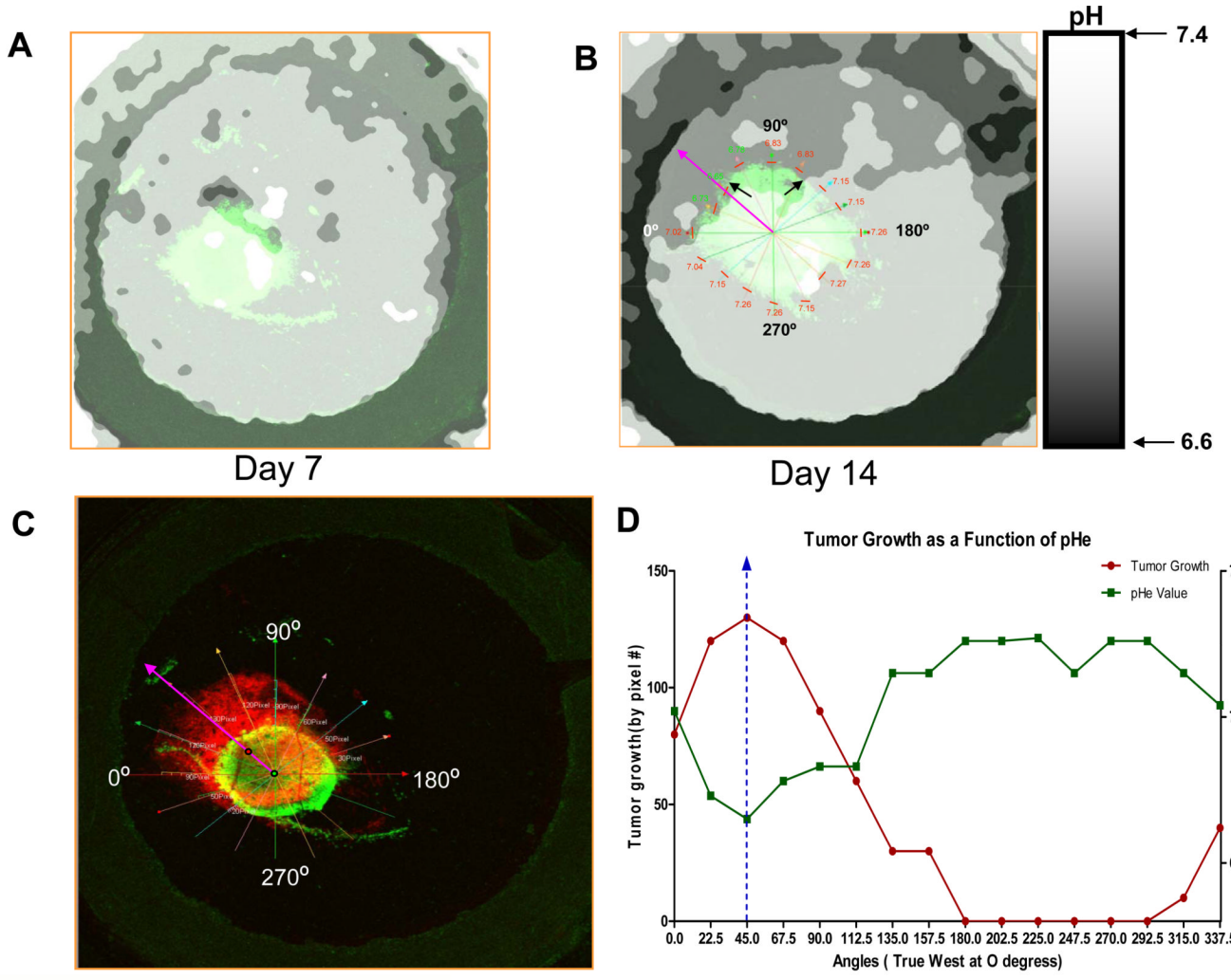

Figure 2. Intravital and ratiometric images of the extracellular pH with SNARF-1

Data are shown for one tumor, which was representative of four control tumors. The extracellular pH (pHe) of HCT116-GFP tumors were measured using SNARF-1 Free Acid at (A) day 7 and (B) day 14. 200μl of 1mmol/L of SNARF solution was injected into the mice via tail vein injection. Images were captured using a 1.25X lens, 50 minutes post SNARF-1 injection. The pHe was measured and ratiometric images were converted to a pH image using calibration data as per Material and Methods. Black arrows are indicating the acidic environment towards which the tumor is growing. In figure (B), the day 14 ratiometric image was co-registered with its corresponding fluorescence image. The pHe was then measured 100microns from the tumor edge (represented by the short red lines). pHe measurements were taken every 22.5 degrees of arc and are located above red lines. Purple arrow indicates the region of strongest acidity and direction of tumor growth. (C) Tumor at day 14 was pseudo-colored red in order to superimpose the tumor image on Day 4 (green) and measure tumor growth from tumor edge on Day 4 to tumor edge on Day 14. Radial lines designate angles and tumor growth was measured by pixels. (D) Tumor growth and pHe plotted as a function of angle.

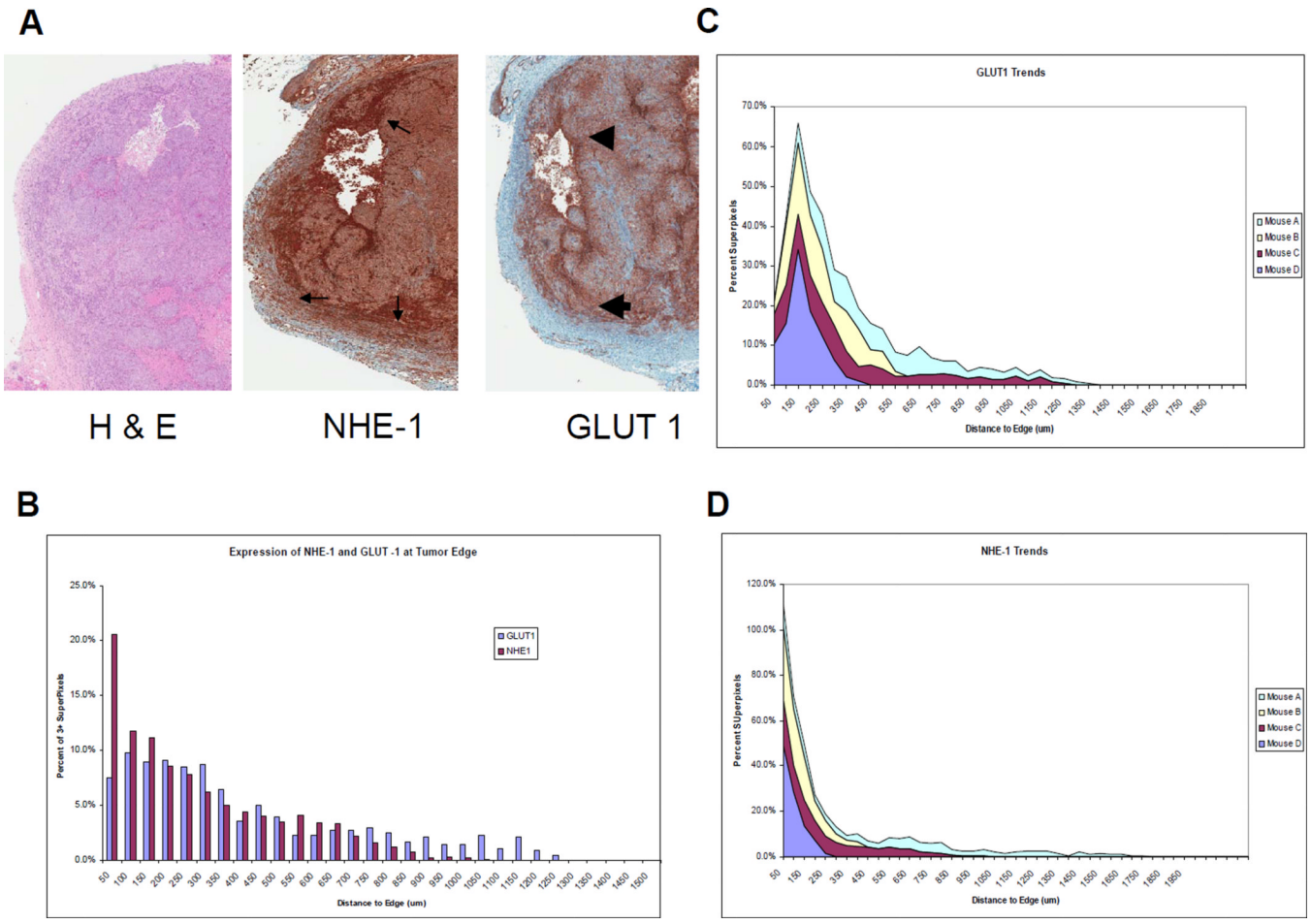

Figure 3. Histology of HCT116/GFP tumors

(A) The tumor edge has an increased expression of NHE-1 (small thin arrows) and GLUT1 (large arrows), which is indicative of acidification caused by an increase in glycolysis. This is consistent with microenvironmental acidosis observed *in vivo* leading to subsequent invasion. (B) Expression of GLUT-1 and NHE-1 as a function of distance from the tumor edge. (C) and (D) Expression trends of GLUT-1 and NHE-1 as a function of distance from tumor edge in N=4 tumors.

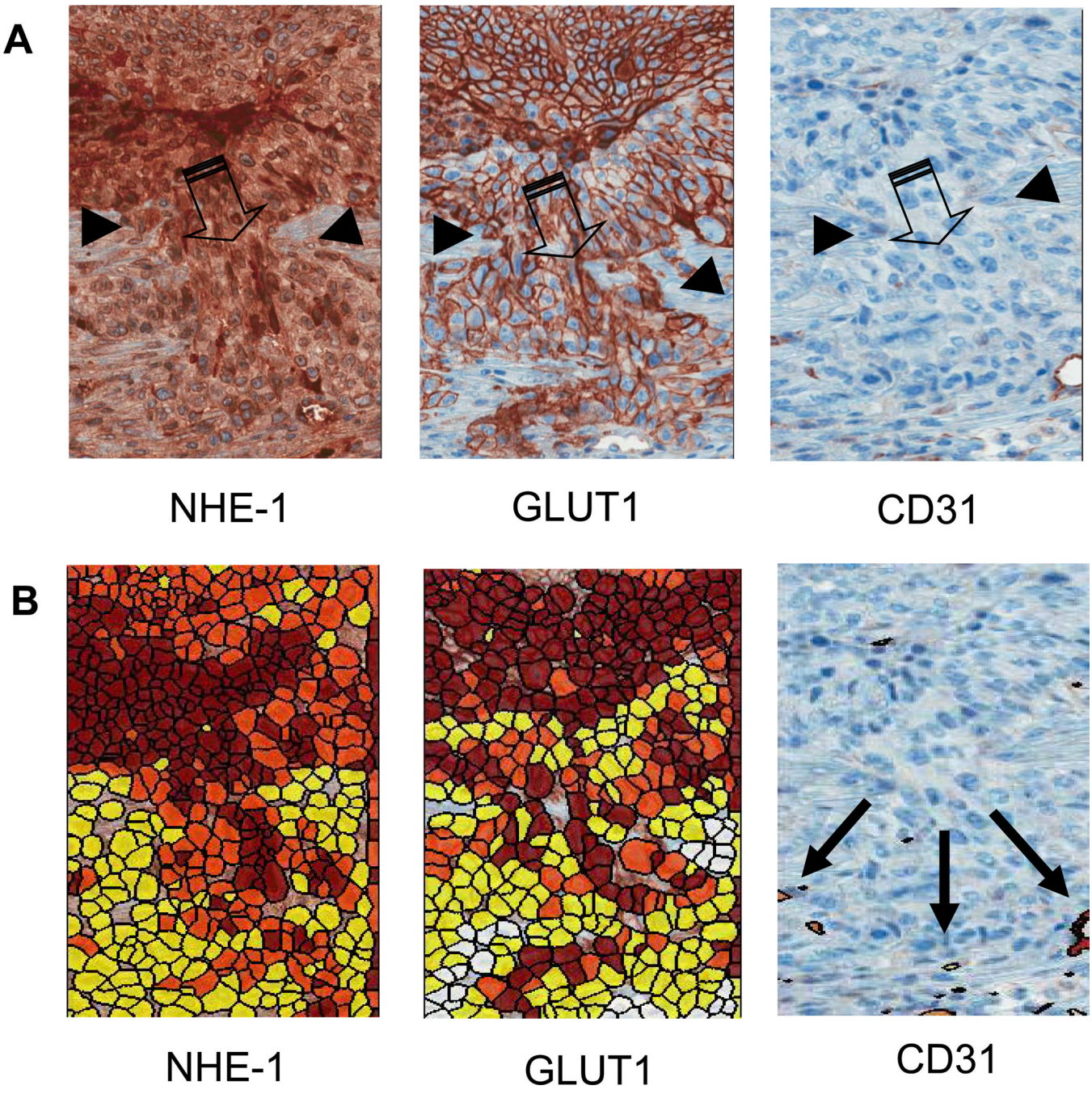

Figure 4. Histology of the invasive edge

(A) Upregulation of NHE-1 exchangers and GLUT-1 are demonstrated by a darker staining of the tumor cells at the invasive front, consistent with an increase in glycolysis and acidosis. CD31 staining is low, suggesting poor perfusion and hence a potential for hypoxia. Images illustrate a region of the tumor edge (small thin arrows) invading into the peritumoral normal tissue (large arrows). (B) Expression of tumor markers GLUT-1, NHE-1, and CD31 were quantified on a per-cell basis (see Methods). Red indicates strong staining, orange is moderate and yellow is weak.

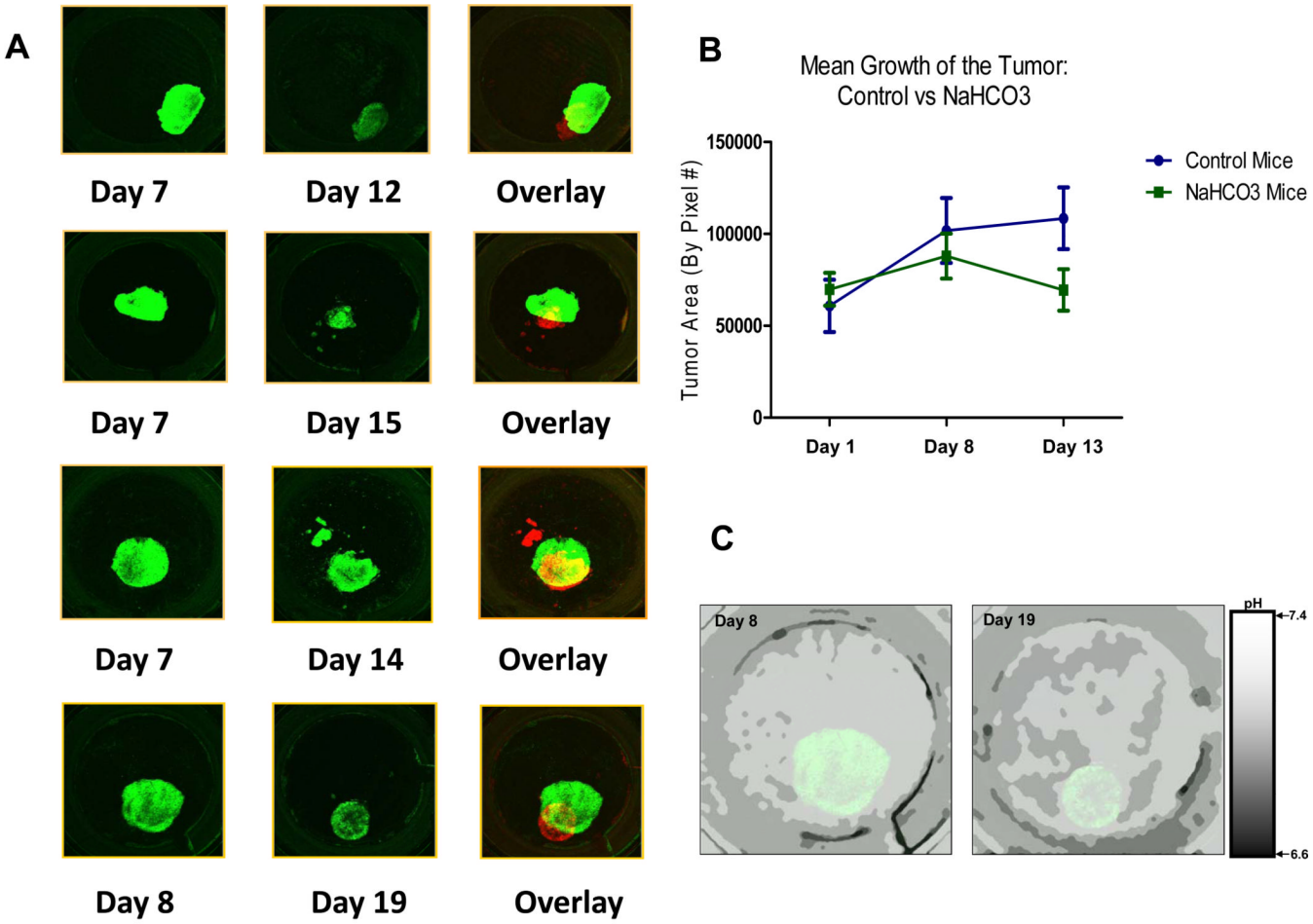

Figure 5. Effects of $NaHCO_3$

(A) Images were captured with a 1.25X lens, showing how we tracked the growth of HCT116-GFP tumors that were treated with 200mmol/L of $NaHCO_3$. Tumor at day 12, 14, 15 and 19 were pseudo-colored red in order to superimpose the images and demonstrate a decrease in tumor size. Images were captured using the Olympus FV1000 MPE laser scanning microscope. (B) Mean area of bicarbonate-treated and control tumors (in pixel count) on days 1, 8 and 13. (C) pHe images of bicarbonate-treated tumors on days 8 and 19. Mice were treated with $NaHCO_3$ as per Materials and Methods. The pHe of HCT116-GFP tumors were measured using SNARF-1 free Acid at day 8 and day 19. 200μl of 1mmol/L of SNARF solution was injected into the mice via tail vein injection. Confocal images were captured 50 minutes post SNARF-1 injection. The pHe was measured and ratiometric images were converted to a pH image using calibration data as per Material and Methods

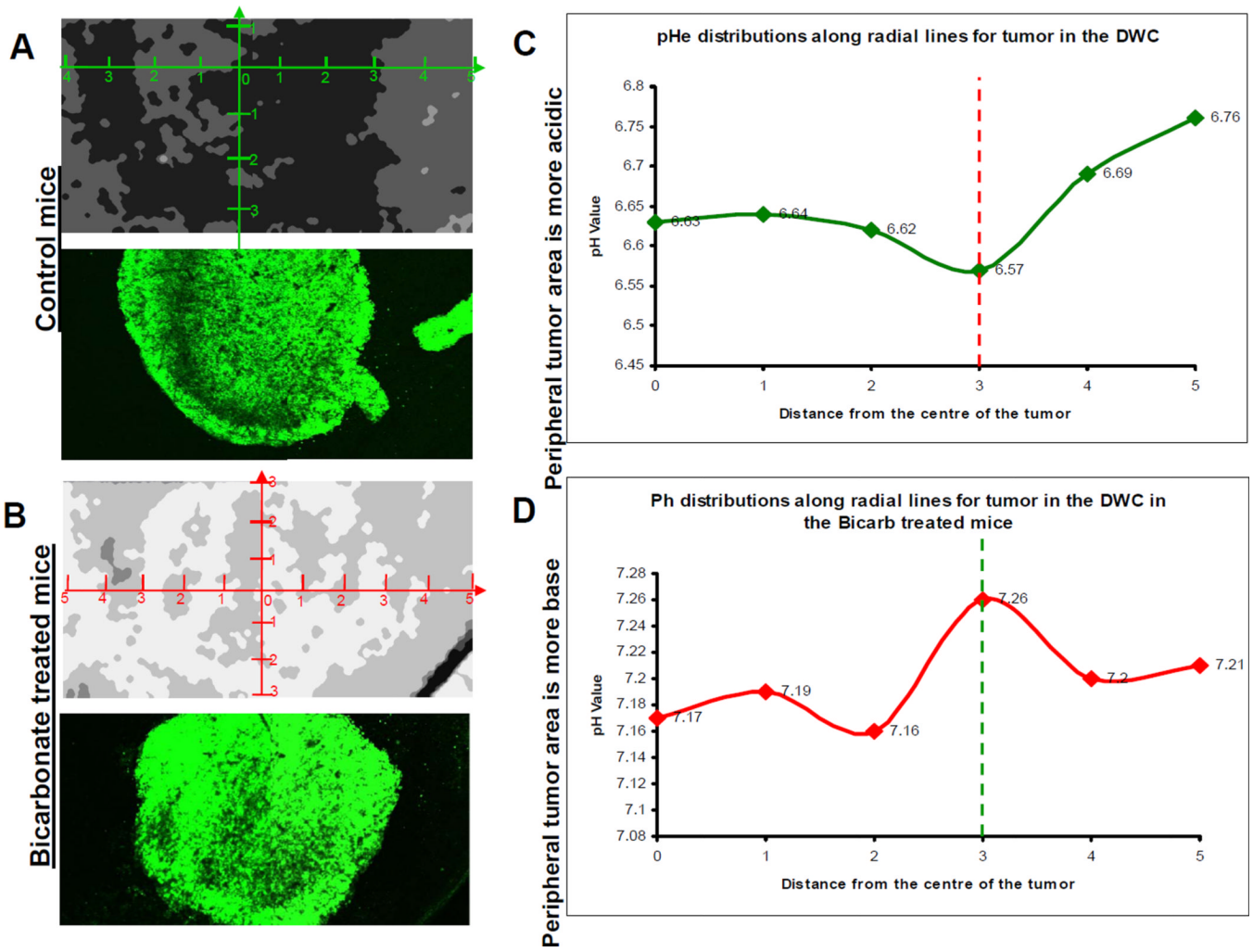

Figure 6. The effect of $NaHCO_3$ treatment on tumor pH

A and B) Ratiometric images from SNARF-1 analysis were used to measure and compare the pH of control tumors to those tumors that were treated with 200mmol/L of $NaHCO_3$. *In vitro* pH calibration was applied to the ratiometric image. pHe profiles, that originated from the center of the tumor, were obtained using a radial graph. pHe values were obtained along the radial lines and the margins of the tumors were defined using GFP images of the tumor. C and D) Least-square fit across all directions and all tumors showing pHe distributions along radial lines. “0” is centroid of tumor in this image. The vertical line indicates tumor edge. Peripheral tumor area is more acidic.